Spatio-temporal variations of seismic coupling along a transform fault: the western North Anatolian Fault Zone

Amandine Amemoutou, Patricia Martínez-Garzón, Virginie Durand, Grzegorz Kwiatek, Marco Bohnhoff, Georg Dresen

Geophysical Journal International

Geophys. J. Int. (2023) **235,** 1982–1995
Advance Access publication 2023 September 06
GJI Seismology

https://doi.org/10.1093/gji/ggad341

Spatio-temporal variations of seismic coupling along a transform fault: the western North Anatolian Fault Zone

Amandine Amemoutou,[1] Patricia Martínez-Garzón,[1] Virginie Durand,[1,*] Grzegorz Kwiatek,[1] Marco Bohnhoff[1,2] and Georg Dresen[1]

[1]*Helmholtz Centre Potsdam, GFZ German Research Centre for Geosciences, Section* 4.2*: Geomechanics and Scientific Drilling, Telegrafenberg,* 14473 *Potsdam, Germany. E-mail: patricia@gfz-potsdam.de*
[2]*Institute of Geological Sciences, Free University of Berlin, Department of Geophysics, 12249 Berlin, Germany*

Accepted 2023 September 5. Received 2023 August 1; in original form 2023 April 26

SUMMARY

The Main Marmara Fault (MMF) forms a major segment of the North Anatolian Fault Zone (NAFZ) in northwestern Türkiye. The MMF represents a seismic gap with currently high seismic hazard and associated risk for the Istanbul metropolitan area. Here we estimate the seismic coupling defined as the ratio of the seismic strain rate to the tectonic strain rate, for the MMF and adjacent NAFZ segments. This ratio indicates the fraction of total strain accumulated with time that is released seismically. We compare the results of seismic strain rates and coupling estimated from earthquakes included in historical and instrumental catalogues, which allows us to identify fault segments that represent a considerable seismic threat during the current seismic cycle. We find that along the main fault traces hosting the large events, seismic strain rates from the historical catalogue are of the same order as the tectonic strain rates. In contrast, coupling estimates based on seismic data from the instrumental catalogue covering also off-fault areas, are up to 100 times smaller, highlighting that most of the seismic energy is released in large earthquakes with recurrence times longer than the time covered by the instrumental catalogue. Within the Sea of Marmara, a significant portion (48%) of shear strain from the instrumental catalogue is currently being accommodated by seismic deformation. Significant variations of the seismic coupling are observed before and after the 1999 $M > 7$ Izmit earthquake, highlighting the different contribution of aseismic slip over different portions of the seismic cycle. A comparison of the temporal evolution of the 1999 Izmit and Düzce post-seismic deformation with seismic strain rates shows that the largest seismic strain rates coincide with the largest post-seismic deformation.

Key words: Earthquake interaction, forecasting and prediction; Seismicity and tectonics; Transform faults; Seismic strain accumulation.

1 INTRODUCTION

During the interseismic period of the seismic cycle, locked faults and their surroundings accumulate elastic strain. As first put forward by Reid (1910), an earthquake may occur due to the sudden release of elastic strain energy stored in response to tectonic loading. Shear stresses on locked faults continuously increase, leading to dynamic fault rupture and the occurrence of an earthquake once the frictional strength of the fault is exceeded (Reid 1910; Thatcher & Rundle 1979; Savage 1983; Cattin & Avouac 2000; Meade & Hager 2005; Sieh *et al.* 2008). While interevent times and coseismic energy release (i.e. magnitude) can vary, in the long run the average cumulative strain energy released by seismic and aseismic slip along a fault and off-fault will amount to the total elastic strain energy fed into the fault system and surroundings through tectonic plate movement. Plate boundaries release energy across a broad spectrum from seismic to slow and aseismic deformation (e.g. Peng & Gomberg 2010). In addition, slip modes may differ over longer timescales along the same fault branch due to geometrical complexities, evolution of fault rocks, varying pore fluid pressures or variations in the loading rate (e.g. McLaskey & Yamashita 2017; Romanet *et al.* 2018). The total strain rate from tectonic loading, $\dot{\varepsilon}_T$, may be expressed as the sum of the strain rate released seismically ($\dot{\varepsilon}_S$), the strain rate released through aseismic slip ($\dot{\varepsilon}_{AS}$) and the

*Now at: Université Côte d'Azur, IRD, CNRS, Observatoire de la Côte d'Azur, Géoazur.

elastic strain rate deforming the fault zone and surrounding crust ($\dot{\varepsilon}_{ACC}$):

$$\dot{\varepsilon}_T = \dot{\varepsilon}_S + \dot{\varepsilon}_{AS} + \dot{\varepsilon}_{ACC} . \quad (1)$$

Seismic coupling has been defined as the ratio of the observed seismic slip rate of a fault and the GPS-derived plate tectonic velocities of the adjacent fault blocks (Pacheco *et al.* 1993; Scholz & Campos 1995, 2012). Spatial variations of seismic coupling are typically recovered for different fault segments or different areas of subduction zones (e.g. Lindsey *et al.* 2021). A key assumption is that interseismic strain accumulation occurs at constant rate and is entirely elastic (Scholz & Campos 2012). However, seismic coupling may vary with time, as is found along simulated seismic cycles in rock deformation experiments, where the seismic coupling tends to increase or decrease as failure approaches, depending on structural fault properties such as roughness (Dresen *et al.* 2020).

Aseismic or slow deformation typically manifests as transients of varying durations (Jolivet & Frank 2020) revealed by geodetic data. Geodetic techniques such as Global Navigation Satellite System (GNSS) and interferometric synthetic aperture radar (InSAR) allow reliable and precise quantification of the interseismic surface displacement. These techniques allow highlighting a fully or partially locked state of a fault where adjacent wall rocks accumulate elastic strain, or steady deformation occurring in the fault zone through aseismic slip. However, for submarine fault segments, GNNS techniques are limited due to absence of near-fault on-land stations and InSAR cannot be applied. Seafloor geodetic measurements along submarine faults are possible in general, but they are costly and their resolution is limited (e.g. Lange *et al.* 2019; Yamamoto *et al.* 2019). Therefore, detailed analysis of the elastic strain released seismically and the subsequent quantification of the seismic coupling is one of the few available options to quantify seismic and aseismic slip.

To estimate seismic coupling, a seismicity catalogue covering the entire seismic cycle of the fault is required. However, the instrumental period in seismology covers only about 120 yr and major earthquakes typically have longer recurrence times (Ben-Zion 2008). Selected portions of the North Anatolian Fault Zone (NAFZ) in Türkiye have an exceptionally complete history of records reflecting the seismicity from the region due to its long settlement history, dating back to 600 BC. Hence, a detailed spatio-temporal analysis of the seismic coupling may help to identify which fault segments are more prone to release a large proportion of seismic waves in an earthquake.

We first estimate the seismic coupling along distinct segments of the western NAFZ using an historical earthquake compilation of the NAFZ covering 2300 yr (Bohnhoff *et al.* 2016a) and a more detailed instrumental seismicity catalogue from KOERI[1] covering the last 120 yr. We then analyse spatio-temporal variations of seismic coupling, focusing on time periods before and after large local earthquakes. Finally, we studied the temporal evolution of the seismic strain rates along the combined 1999 Izmit–Düzce rupture and compared it to the evolution of the post-seismic deformation after the $M > 7$ earthquakes.

[1]Kandilli Observatory and Earthquake Research Institute in Istanbul (http://www.koeri.boun.edu.tr/sismo/2/earthquake-catalog/, last accessed 05/02/2023).

2 RECENT LARGE EARTHQUAKES ON THE NORTH ANATOLIAN FAULT ZONE AND PREVIOUS SEISMIC COUPLING ESTIMATES

The NAFZ is one of the best-studied continental transform fault zones with first reports written by Ketin (1948). Starting in 1939 with the Erzincan M_w 7.9 earthquake, a sequence of large-magnitude ($M > 7$) earthquakes propagated westwards, with the most recent earthquakes being the 1999 M_w 7.4 Izmit and M_w 7.1 Düzce occurring east of the Sea of Marmara (Pinar *et al.* 2001; Barka *et al.* 2002; Bohnhoff *et al.* 2016b). Together with the 1912 Ganos/Murefte M_w 7.4 earthquake in western Marmara, the entire NAFZ ruptured in $M > 7$ earthquakes in the 20th century except for the Main Marmara Fault below the Sea of Marmara (MMF) which is considered a seismic gap that is partly locked (Bohnhoff *et al.* 2013; Ergintav *et al.* 2014; Becker *et al.* 2023). There, the last major (M 7.4) earthquake occurred in 1766. Considering an average recurrence time of 250 yr, the MMF is late in its seismic cycle and the probability for a $M > 7$ earthquake over the next 50 yr is 35–70 per cent (Parsons 2004; Murru *et al.* 2016).

Previous estimates of the seismic coupling for this region used broadly spaced geodetic data to compare geodetic and seismic strain rates. Ward *et al.* (1998) used the seismicity catalogue available from the National Earthquake Information Center and estimated the scalar version of Kostrov's (1974) earthquake moment rates, recovering a seismic coupling of 22 per cent for the entire Anatolia. Jenny *et al.* (2004) used published GPS measurements and several seismicity catalogues to map geodetic strain rates, and reported moderate to large seismic coupling along the western segments of NAFZ. More recently, Sparacino *et al.* (2022) evaluated seismic and geodetic moment rates around the entire Mediterranean region, and obtained a seismic coupling of about 20 per cent for the Marmara region, and up to 50 per cent for the Izmit–Düzce region further east. All these studies were performed over scales covering thousands of km, while a detailed estimation is missing.

The MMF extends between the Ganos segment west of the Tekirdağ Basin and the Gulf of Izmit at the western tip of the 1999 Izmit rupture (Fig. 1). The fault is assumed to accommodate most of the regional deformation with rates of about 20 mm yr^{-1} (Hergert & Heidbach 2010; Ergintav *et al.* 2014). The segment extending through the Gulf of Gemlik (Le Pichon *et al.* 2001, see Fig. 1 for location) is part of the southern NAFZ branch, where fault slip rates are about 5 mm yr^{-1} (Ergintav *et al.* 2014).

The westernmost NAFZ segment analysed in this study includes the eastern part of the Ganos segment and the Tekirdağ Basin (GN and TB, Fig. 1a). The Ganos fault ruptured last in 1912 with a M_w7.4 earthquake. InSAR analysis evidenced a locked state of its onshore portion (Motagh *et al.* 2007) in accordance with the absence of local seismicity (e.g. Janssen *et al.* 2009). East of the Tekirdağ Basin the Western High and the Central Basin (WH and CB, Fig. 1) represent a wider fault zone, accommodating the shape of the basin and the seismicity follows the mapped fault segments (Wollin *et al.* 2018). Recently, earthquake repeaters have been identified in this part, suggesting that the tectonic strain is partially released aseismically through fault creep (Schmittbuhl *et al.* 2015, 2016; Bohnhoff *et al.* 2017a; Uchida *et al.* 2019; Becker *et al.* 2023). This is also supported by seafloor geodetic measurements (Yamamoto *et al.* 2019). The Kumburgaz Basin (KB, Fig. 1) is located directly east of the Central Basin. The seismic activity is lower in this area compared to the Tekirdağ and Central Basins (Schmittbuhl *et al.* 2015; Martínez-Garzón *et al.* 2019). Seafloor acoustic techniques evidenced that the

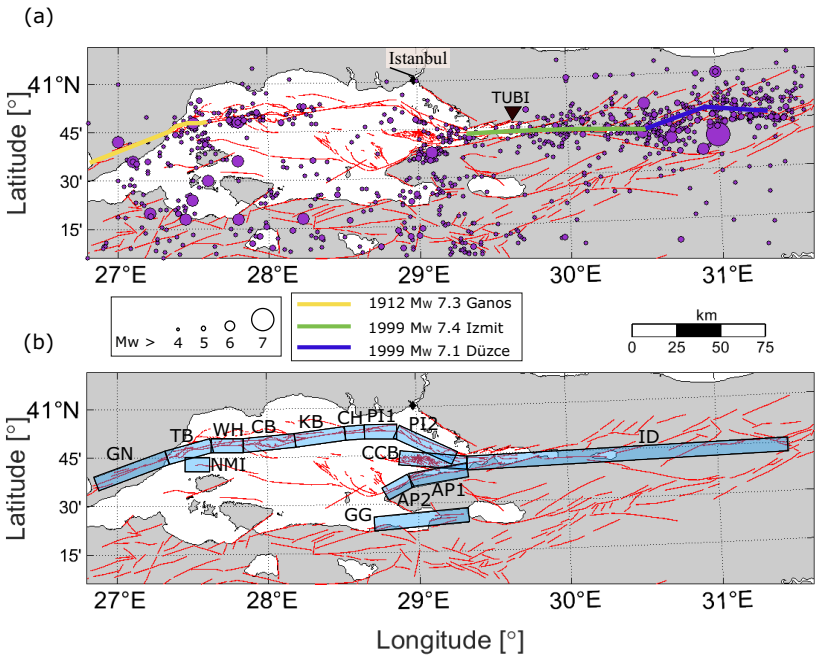

Figure 1: The NAFZ in northwestern Türkiye. (a) Map of the $M_w \geq 4$ instrumental seismicity catalogue (KOERI, purple circles) from January 1900 to April 2021. Symbol size is encoded with M_w. The 1912 M_w 7.4 Ganos 1999 M_w7.4 Izmit and 1999 M_w 7.1 Düzce ruptures are marked with yellow, green and blue lines, respectively. Black downward triangle shows the GPS station TUBI (Section 4.4). (b) Spatial extension of the 14 segments studied. The red lines indicate mapped fault segments (Emre *et al.* 2013). GN: Ganos fault, TB: Tekirdağ Basin, WH: Western High, CB: Central Basin, KB: Kumburgaz Basin, CH: Central High, PI: Princes' Island, CCB: Çınarcık Basin, AP: Armutlu Peninsula, GG: Gulf of Gemlik, NMI: North of Marmara Island, ID: Izmit–Düzce.

Kumburgaz segment is fully locked (Sakic *et al.* 2016; Lange *et al.* 2019). The Princes Island segment (PI1 and PI2, Fig. 1) is the easternmost part of the MMF and it is located the closest to the Istanbul urban area. This segment was identified to be fully locked down to about 10 km based on absent seismicity (Bohnhoff *et al.* 2013) and from onshore GPS measurements (Ergintav *et al.* 2014). The Armutlu peninsula forming the southern shore of the eastern Sea of Marmara hosts a hydrothermal system, with higher seismic activity. There, the largest earthquake occurred in 1963 with a M_S 6.3, and numerous aftershocks occurred here following the 1999 Izmit earthquake (Bohnhoff *et al.* 2006; Durand *et al.* 2010). The region also experiences episodic shallow slow-slip events associated with moderate seismicity indicating a complex local interaction of seismic and aseismic energy release (Martínez-Garzón *et al.* 2019, 2021; Durand *et al.* 2022). Below the Izmit Bay, the MMF connects with smaller branches of the main northern NAFZ branch (including the Armutlu fault, see Fig. 1) then forming the single northern NAFZ branch along the Izmit and Düzce sections that ruptured in 1999. Towards the east, seismicity spreads over a large area off the segmented fault trace, signifying a wide fault zone surrounding the fault core (Ben-Zion & Sammis 2003).

3 DATA AND METHODS

3.1. Historical and instrumental earthquake catalogues

We utilized the instrumental seismicity catalogue covering 120 yr available from KOERI as well as the refined historical earthquake catalogue for the entire NAFZ spanning 2300 yr from Bohnhoff *et al.* (2016a). The study region was divided into 14 fault sections (Fig. 1).

The instrumental KOERI catalogue for the study region [27°–31.5°E, 40.3°–41.1°N] spans from January 1900 to April 2021. The magnitude type includes short-period body wave (M_b), duration (M_d), local (M_L), surface wave (M_S) and moment (M_w) magnitudes. We homogenized all the magnitudes to M_w. For earthquakes with $M < 4$ and no M_w available in the catalogue, we assumed $M_L \approx M_w$ following Kılıç *et al.* (2017). For earthquakes $M \geq 4$ (Fig. 1), we followed the orthogonal regression equation for M_S to M_w and the ordinary least squares regression equations for M_b, M_d, M_L to M_w in the Marmara region defined by Kadirioğlu & Kartal (2016) (see text in Supplement S1). After conversion, the magnitudes cover the range M_w [0.2–7.4]. After removing the events labelled as quarry blasts by KOERI a total of 21 245 earthquakes remained for further analysis.

The historical seismicity catalogue from Bohnhoff *et al.* (2016a) is a compilation of different earthquakes and catalogues available from literature and includes 77 earthquakes with $M_S > 5.8$ along the NAFZ and surrounding area. Magnitudes were converted into M_S following the relation from Scordilis (2006). The catalogue covers 2300 yr, and therefore about nine seismic cycles assuming a recurrence interval of about 250 yr for M_w 7–7.5 earthquakes in NW Türkiye (Parsons *et al.* 2004; Murru *et al.* 2016). It has an estimated magnitude of completeness $M_c = 7.3$ and includes 14 events with $M_S \geq 7.3$ (Bohnhoff *et al.* 2016a). We also converted M_S to M_w using the same relations described above. As the instrumental seismicity catalogue starts in the year 1900, we ended the historical catalogue in the year 1900.

3.2. Tectonic strain rate $\dot{\varepsilon}_T$

We estimated the tectonic shear strain rate $\dot{\varepsilon}_T$ as the long-term fault slip rate $\dot{S}$ divided by the damage zone width W measured normal

to the fault trace over which the deformation is accommodated:

$$\dot{\varepsilon}_{\mathrm{T}} = \frac{\dot{S}}{W}\,. \tag{2}$$

Numerous studies have determined slip rates along the NAFZ based on different methodologies. We mostly used the geodetic long-term slip rates from Ergintav *et al.* (2014) and those derived from geomechanical modelling of the Marmara region (Hergert & Heidbach 2010). The largest slip rates are observed in the Izmit–Düzce region with 25 mm yr^{-1} and along the Ganos fault with 20 mm yr^{-1} (see Table 1). We utilized the strain rates instead of the direct estimations of the slip rate to more specifically address the variable width over which the tectonic deformation is accommodated along the fault. The W for each fault segment was calculated as the distance from the surface fault trace containing either 68 or 95 per cent of the seismicity (Figs 2 and 3).

3.3 Seismic strain rate $\dot{\varepsilon}_{\mathrm{S}}$

We follow Kostrov (1974) and Brune (1968) and estimated the seismic strain rates $\dot{\varepsilon}_{\mathrm{S}}$ from total seismic moment M_0 released in N earthquakes occurring in a certain crustal volume V during time period T:

$$\dot{\varepsilon}_{\mathrm{S}} = \frac{1}{2\mu V T}\sum_{n=1}^{N} M_{\mathrm{O}}, \tag{3}$$

where μ is the shear modulus, typically assumed $\sim 3 \times 10^{10}$ Pa. We calculated M_0 [N m] following Hanks & Kanamori (1979):

$$M_0 = 10^{\frac{3}{2}M_{\mathrm{w}}+9.1}. \tag{4}$$

We divided our study region into volumes V of $2 \times 2 \times 15$ km^3, (with 15 km being the depth dimension), and calculated the seismic strain rates $\dot{\varepsilon}_{\mathrm{S}}$ for each V. The size of the horizontal dimension was chosen considering the uncertainties of the epicentral locations observed in the region, and the depth range represents approximately the seismogenic thickness from the seismicity distribution (Wollin *et al.* 2018; Meghraoui *et al.* 2021; Karabulut *et al.* 2011; Schmittbuhl *et al.* 2016). ΔT corresponds to the time span covered by the corresponding seismicity catalogue, (i.e. 120 and 2300 yr for the instrumental and historical catalogues, respectively).

To avoid concentrating the energy released through $M_{\mathrm{w}} \geq 4$ earthquakes (typically with surface rupture lengths SRL > 2 km) into only one V, we compiled a database of available focal mechanisms from different studies in the region (Pinar *et al.* 2003; Örgülü *et al.* 2011; Öztürk *et al.* 2015; Coskun *et al.* 2017; Wollin *et al.* 2018) and applied the following methodology to each $M_{\mathrm{w}} \geq 4$ event: (1) we attributed a focal mechanism to the event (see Fig. S1). If no focal mechanism was available, we associated it with the focal mechanism of the closest event in space with the focal mechanism available. (2) We calculated the SRL [km] according to their M_{w}:

$$\mathrm{SRL} = 10^{(a+b*\mathrm{M_W})} \tag{5}$$

where $a = -3.55$ and $b = 0.74$ following Wells & Coppersmith (1994). (3) We created 1000 points distributed uniformly along the SRL with the orientation of the corresponding fault strike for the focal mechanism (see Fig. S2). (4) We distributed the M_0 of the event uniformly over 1000 points spanning its entire rupture length, so that the sum of all the seismic moments is equal to the seismic moment of the event.

3.4 Seismic coupling χ_{S}

We define seismic coupling χ_{S} as (Pacheco *et al.* 1993; Scholz & Campos 1995):

$$\chi_{\mathrm{S}} = \frac{\dot{\varepsilon}_{\mathrm{S}}}{\dot{\varepsilon}_{\mathrm{T}}}\,. \tag{6}$$

Seismic coupling approaching unity indicates that tectonic deformation is accommodated almost entirely by seismic slip. Conversely, if seismic coupling tends to zero, either the fault deforms aseismically (through steady-state creep or episodic slow-slip events) or, alternatively, the fault is locked accumulating elastic strain (Scholz & Campos 2012). Stored elastic strain available to rupture in future earthquakes may be estimated from comparing total (aseismic and seismic) slip rate accommodated by a fault and surrounding damage zone to the relative velocity of bounding plate segments (Carafa *et al.* 2017).

Note that our seismic coupling definition is slightly different than geodetic coupling. Geodetic coupling reflects whether a fault is locked or accommodating displacement (e.g. Radiguet *et al.* 2016; Lindsey *et al.* 2021), whereas our estimated seismic coupling reflects strictly how seismically active the fault has been over the analysed time period.

4 RESULTS

4.1 Width of the deformation zone W and tectonic strain rates $\dot{\varepsilon}_{\mathrm{T}}$

The estimated W varies from 4.5 km in the Çınarcık Basin to 15.3 km in the Izmit–Düzce region (Figs 2 and S1, Table 1). Nevertheless, the $\dot{\varepsilon}_{\mathrm{T}}$ remained within the same order (0.1–1 μstrain yr^{-1}) throughout the entire study region (Fig. 3). This general trend is stable with respect to utilizing 68 or 95 per cent of the seismicity distribution from the fault trace (Fig. 3). The maximum $\dot{\varepsilon}_{\mathrm{T}} = 1.6$ μstrain yr^{-1} is obtained in the Central High region of the Marmara Sea (Table S1). The $\dot{\varepsilon}$ in the Izmit–Düzce segment is slightly lower than average ($\dot{\varepsilon}_{\mathrm{T}} = 0.8$ μstrain yr^{-1}, see Table S1), which is likely linked to the larger W obtained for this segment (Table 1). This may result from a wide off-fault damage zone surrounding the fault and from the Düzce fault dipping about 60° towards North. Compared to the regions located in the MMF, the faults on Armutlu peninsula, the area north of Marmara Island and the southern branch along the Gulf of Gemlik (see Fig. 1 for locations) show smaller $\dot{\varepsilon}_{\mathrm{T}}$ of about 0.1 μstrain yr^{-1}, in agreement with the smaller slip rates accommodated by these fault segments (Fig. 3 and Table 1).

4.2 Seismic strain rates and coupling from historical and instrumental catalogues

The seismic strain rates calculated from the instrumental seismicity catalogue ($\dot{\varepsilon}_{\mathrm{S}}^{\mathrm{inst}}$) span from 10^{-14} to 10^{-5} strain yr^{-1}, with a median ($\dot{\varepsilon}_{\mathrm{S}}^{\mathrm{inst}}$) $= 2 \times 10^{-9}$ strain yr^{-1} (Fig. 4a and Table S2). The seismic strain rates estimated with the historical seismicity catalogue ($\dot{\varepsilon}_{\mathrm{S}}^{\mathrm{hist}}$) yield a comparatively smaller span of values from 10^{-8} to 10^{-5} strain yr^{-1} with a median($\dot{\varepsilon}_{\mathrm{S}}^{\mathrm{hist}}$) $= 4 \times 10^{-7}$ strain yr^{-1} (Fig. 4a and Table S2). This value is of the same order as the median tectonic strain rate median ($\dot{\varepsilon}_{\mathrm{T}} = 10^{-7}$, see Fig. 4a). The median ($\dot{\varepsilon}_{\mathrm{S}}^{\mathrm{inst}}$) is about two orders smaller than the median ($\dot{\varepsilon}_{\mathrm{S}}^{\mathrm{hist}}$). As the median $\dot{\varepsilon}_{\mathrm{S}}$ value from each catalogue is calculated from the bins that contain seismicity, the difference between the two values is partially caused by the lower magnitude of completeness of the

Table 1: Slip rates $\dot{S}$ along the selected segments of the western NAFZ and calculated width of the deformation zone $W_{68\text{ per cent}}$. Fault segments as in Fig. 1(b). 'LON min' and 'LON max' give segment boundaries, respectively.

Fault segments	Abbr.	LON min [°]	LON max [°]	Slip rate $\dot{S}$ [mm yr^{-1}]	References	$W_{68\text{ per cent}}$ [km]	$W_{95\text{ per cent}}$ [km]
Ganos	GN	27.06	27.33	20	Ergintav *et al.* 2014	8.4	15.7
Tekirdağ Basin	TB	27.33	27.63	15.5	Hergert & Heidbach 2010	7.6	13.6
Western High	WH	27.62	27.84	16		5.7	15.5
Central Basin	CB	27.84	28.2	15.5		7.2	16.4
Kumburgaz Basin	KB	28.19	28.52	16.5		6.2	13.5
Central High	CH	28.52	28.65	15.5		5	9.8
Princes' Island	PI1	28.65	28.86	12.5	Ergintav *et al.* 2014	6.5	13.1
/	PI2	28.86	29.25	12.5		5.8	12.4
Çınarcık Basin	CCB	28.88	29.33	12.5		4.5	7.6
Armutlu Peninsula	AP1	28.95	29.33	6	Bohnhoff *et al.* 2013	6.2	10.8
/	AP2	28.78	28.95	6		5.5	10.6
Gulf of Gemlik	GG	28.71	29.33	2	Ergintav *et al.* 2014	8.3	17.4
North of Marmara Island	NMI	27.45	27.61	1.5		5.8	9.5
Izmit–Düzce	ID	29.40	32.11	25		15.3	27.3

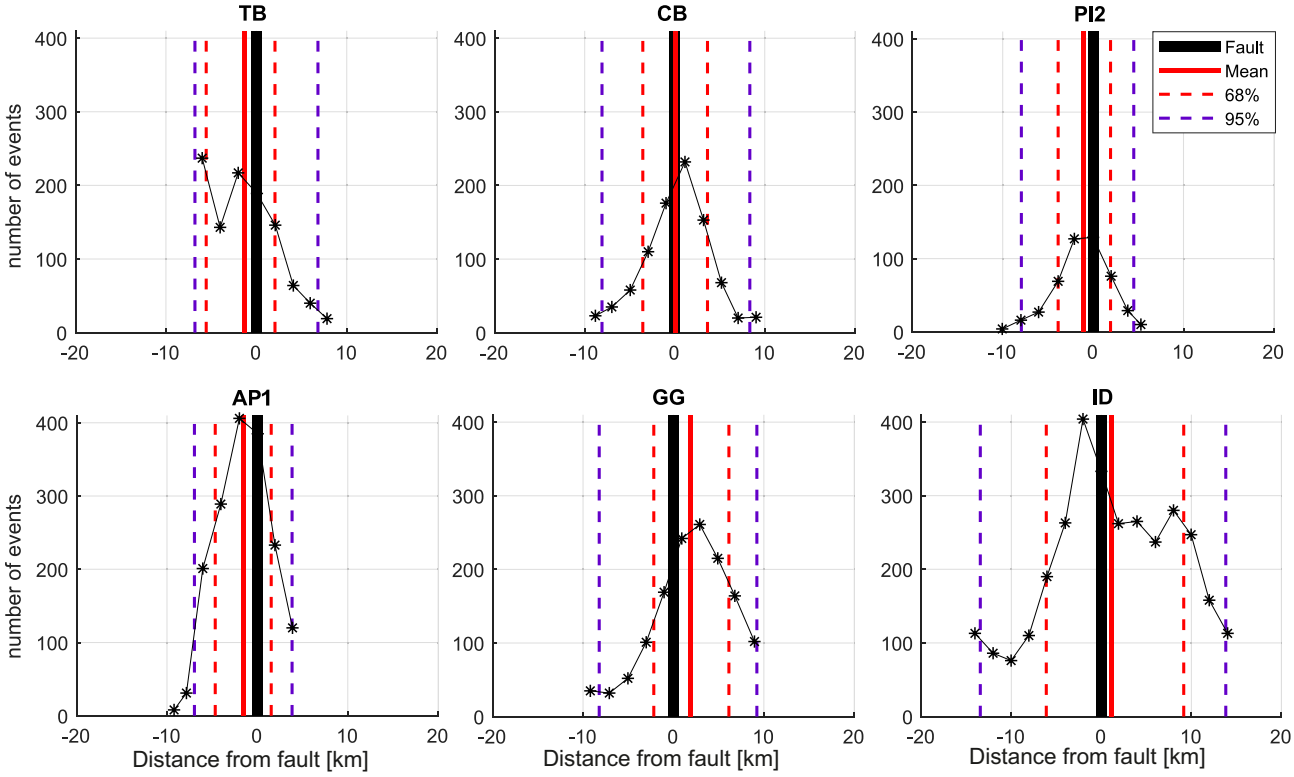

Figure 2: Distribution of the number of seismic events as a function of distance normal to the main surface fault trace for selected fault segments (labelling of fault segments as in Fig. 1 and Table 1). Distributions for remaining segments are provided in Fig. S3. Positive and negative distance values indicate the distance north and south of the fault surface trace, respectively. Red and purple vertical dashed lines represent the epicentral distances normal to the fault trace containing 68 and 95 per cent of the seismic events, respectively.

instrumental catalogue ($M_C = 2.1$). The increased number of bins with small magnitude events from the instrumental catalogue provide higher resolution of low average seismic strain rates along the fault zone compared to the historical catalogue (Fig. 4). In addition, considering the recurrence time of 250 yr of M 7–7.5 events, the instrumental catalogue covers less than half of a seismic cycle in the Sea of Marmara. The larger seismic strain rates from the historical catalogue with respect to the instrumental catalogue suggest that the accumulated elastic strain on the faults is mainly released via large earthquakes, which are not fully present in our instrumental catalogue as it covers less than one entire seismic cycle. The spatial distribution of $\dot{\varepsilon}_S^{inst}$ and $\dot{\varepsilon}_S^{hist}$ shows that values reach a maximum within the mapped fault zones (Figs 4b and c). Segments that hosted the 1912 M_w 7.4 Ganos, 1999 M_w 7.4 Izmit and 1999 M_w 7.1 Düzce earthquakes, display the highest $\dot{\varepsilon}_S^{inst}$. The $\dot{\varepsilon}_S^{hist}$ are also larger along the Ganos and the Izmit–Düzce segments, leaving the Sea of Marmara region with smaller $\dot{\varepsilon}_S^{hist}$ (Fig. 4c).

In the next step, we analysed the seismic coupling (χ_S) distributions using the instrumental and historical seismicity catalogues,

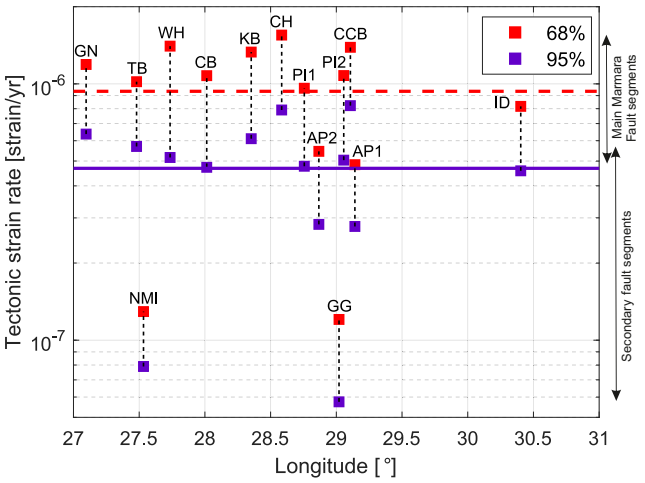

Figure 3: Tectonic strain rates $\dot{\varepsilon}_T$ [strain yr^{-1}] for the selected fault segments (shown with square symbols, see labelling of fault segments in Table 1 and Fig. 1 for locations). Red and blue symbol colours show $\dot{\varepsilon}_T$ values using a W determined from 68% and 95% of the seismicity distribution, respectively. The dashed red and solid blue horizontal lines indicate the average $\dot{\varepsilon}_T$ values using a fault zone width W determined from 68% and 95% of the seismicity distribution, respectively.

separately (Fig. 5). The χ_S^{hist} reach values up to 100 per cent in areas of previous large magnitude earthquakes. Using the ratio median($\dot{\varepsilon}_S^{hist}$)/median($\dot{\varepsilon}_T$), we obtained average seismic coupling values of 48% and 96% for the entire analysed spatio-temporal region when utilizing$W_{68\%}$ and $W_{95\%}$, respectively (Fig. 5a). Hence, these values indicate that 48%–96% of the long-term shear strain accumulated from tectonic loading is accommodated by seismic activity.

As observed with the strain rates, χ_S^{inst} is about two orders smaller than χ_S^{hist} (Fig. 5a). This lower estimate is a result of the overall lower seismic strain rates as described above, partially affected by the larger proportion of smaller seismic events, the lack of large earthquakes and the relatively short time span which does not reflect an entire seismic cycle.

4.3 Spatio-temporal variations of seismic strain rates and coupling related to $M > 7$ earthquakes

Our results show that throughout the seismic cycle, seismic strain rates (and therefore seismic coupling) are not constant. We investigate how the seismic strain rates and seismic coupling varied within the 120-yr time span included in the instrumental catalogue. To this end, we divided the instrumental catalogue into two different temporal periods, the first covering from 1900 until 1 d before the 1999 M_w 7.4 Izmit earthquake ('time period 1', Figs 6a and b), and the second from 2 weeks after the 1999 M_w 7.1 Düzce earthquake (to reduce the effect of aftershocks) until the end of the year 2021 ('time period 2', Figs 6a and c).

The regions with the largest $\dot{\varepsilon}_S^{inst}$ during time period 1 are Ganos and south of Düzce, which hosted large earthquakes in 1912, and 1957 and 1967, respectively. A distinct increase in $\dot{\varepsilon}_S^{inst}$ is observed from time period 1 (median ($\dot{\varepsilon}_S^{inst}$) $= 5 \times 10^{-10}$ strain yr^{-1}) to time period 2 (median ($\dot{\varepsilon}_S^{inst}$) $= 2 \times 10^{-9}$ strain yr^{-1}, Fig. 6a) considering the entire study area. This temporal increase in the $\dot{\varepsilon}_S^{inst}$ illustrates the strong effect that the occurrence of the 1999 $M > 7$ Izmit and Düzce earthquakes imprinted on the seismicity distribution of the broader Marmara region.

In addition to this overall trend of the entire region, we also observe some local $\dot{\varepsilon}_S^{inst}$ decrease from time period 1 to time period 2 (Fig. 6c). This applies specifically to the Izmit segment, where the $\dot{\varepsilon}_S^{inst}$ decreased almost 2 orders from 10^{-6} to 10^{-8}. In this case, we investigated the evolution of $\dot{\varepsilon}_S^{inst}$ by separating into two periods: the first spanning from January 1900 to 1 d before the 1912 M_w 7.4 Ganos earthquake (Figs S4b and S5a), and the second from 2 weeks after the 1912 M_w 7.4 Ganos earthquake up to 1 d before the 1999 M_w 7.4 Izmit earthquake (Figs S4b and S5b). Although the resolution of the instrumental catalogue back to 1900s was clearly lower, the seismic activity and hence seismic strain rates also decreased after the 1912 M_w 7.4 Ganos event around its rupture length.

The calculated χ_S^{inst} between time periods 1 and 2 also show a shift corresponding to the reported variations in the seismic strain rates, with average values around 0.1 per cent before the 1999 M_w 7.4 Izmit and around 1 per cent after the occurrence of the 1999 $M > 7$ Izmit–Düzce sequence over the entire region (Fig. 7a). The areas with lower $\dot{\varepsilon}_S^{inst}$ during time period 1, including segments from Tekirdağ basin to the Gulf of Gemlik in the Sea of Marmara and the area west of Düzce consistently show also lower χ_S^{inst} (Fig. 7b), which increased about two orders during time period 2. Conversely, the Izmit and Düzce areas with higher χ_S^{inst} during time period 1 show a decrease for time period 2. The higher seismic coupling during the years before the 1999 Izmit earthquake reflect that the area was seismically active for several years before it finally ruptured in a large earthquake. In addition, the lower seismic coupling after the 1999 earthquakes could reflect the large stress release in the region, requiring several years to build up sufficient tectonic strain to generate seismicity.

In summary, the occurrence of the 1999 M_w 7.4 Izmit and M_w 7.1 Düzce earthquakes led to larger overall $\dot{\varepsilon}_S^{inst}$ and seismic coupling χ_S^{inst}over the entire analysed area. In contrast the Izmit region displayed locally lower $\dot{\varepsilon}_S^{inst}$.

4.4 Seismic strain rates and post-seismic deformation after the 1999 Izmit–Düzce sequence

Ergintav *et al.* (2009) studied almost 7 yr of the GPS time-series (1998–2007) capturing the post-seismic deformation following the 1999 Izmit–Düzce rupture. We compare the post-seismic slip after the 1999 Izmit earthquake captured with the near-field GPS station TUBI to the temporal evolution of the $\dot{\varepsilon}_S$ in the 1999 $M > 7$ Izmit and Düzce earthquake rupture areas. TUBI is located ~50 km northwest of the 1999 M_w 7.4 Izmit epicentre and is part of the continuously operating GNSS network monitoring the Sea of Marmara (see Fig. 1 for station location). The north (N) and east (E) components of TUBI show three distinct deformation periods related to the 1999 $M > 7$ Izmit–Düzce earthquake sequence (Fig. 8a).

Before the 1999 M_w 7.4 Izmit earthquake, the GPS positions indicate almost no displacements on the N and E components when corrected for interseismic and co-seismic offsets (Fig. 8a). Following the 1999 M_w 7.4 Izmit earthquake recorded displacements accelerated. The east component shows a jump of ~30 mm between the 1999 $M > 7$ Izmit and Düzce earthquakes in agreement with the right lateral slip rate of the NAFZ (Barka 1992; McClusky *et al.* 2000; Reilinger *et al.* 2006) and the time-series reflect a logarithmic evolution as determined by Ergintav *et al.* (2009, Fig. 8a). The occurrence of the 1999 M_w 7.1 Düzce earthquake did not have a remarkable effect on the displacement evolution, which continued

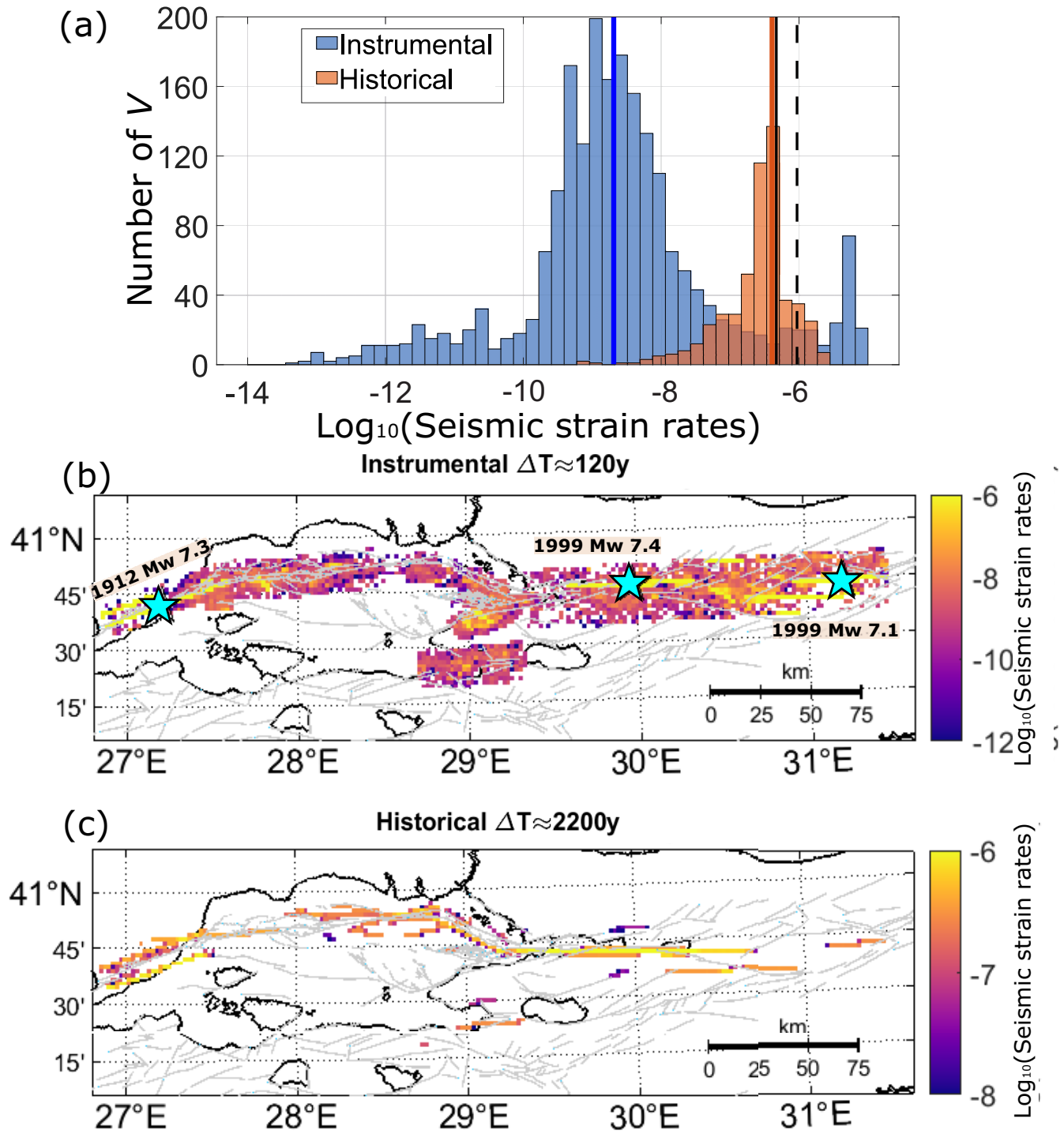

Figure 4: Seismic strain rates calculated for the instrumental and historical seismicity catalogues. (a) Histograms showing seismic strain rates distributions within the estimated volumes V for the instrumental (blue) and historical (orange) catalogues. Vertical blue and orange lines represent the median for the instrumental and historical catalogues, respectively. Vertical black continuous and dashed lines represent the median of tectonic strain rates over the entire region using per cent and per cent, respectively. (b) Spatial distribution of $\dot{\varepsilon}_S^{inst}$. (c) Same as (b) but for $\dot{\varepsilon}_S^{hist}$. Colour bar range is selected to emphasize the changes (see histograms for the complete ranges of values). Light grey lines indicate mapped faults in the studied area.

following a logarithmic trend that started at the time of the Izmit earthquake.

We calculated the temporal evolution of the $\dot{\varepsilon}_S$ from 1998 to 2007 (Fig. 8b), considering the seismicity ($M_w > 2.5$) within the Izmit–Düzce segment (see Fig. 1) using eq. (3) in sliding windows of 80 events with an overlap of 20 events. By comparing the post-seismic deformation of the 1999 Izmit and Düzce earthquakes from the GPS time-series to our $\dot{\varepsilon}_S$, we find that the $\dot{\varepsilon}_S$ evolution closely follows the post-seismic displacement trend induced by the 1999 Izmit–Düzce earthquakes. Before the Izmit earthquake we observed a

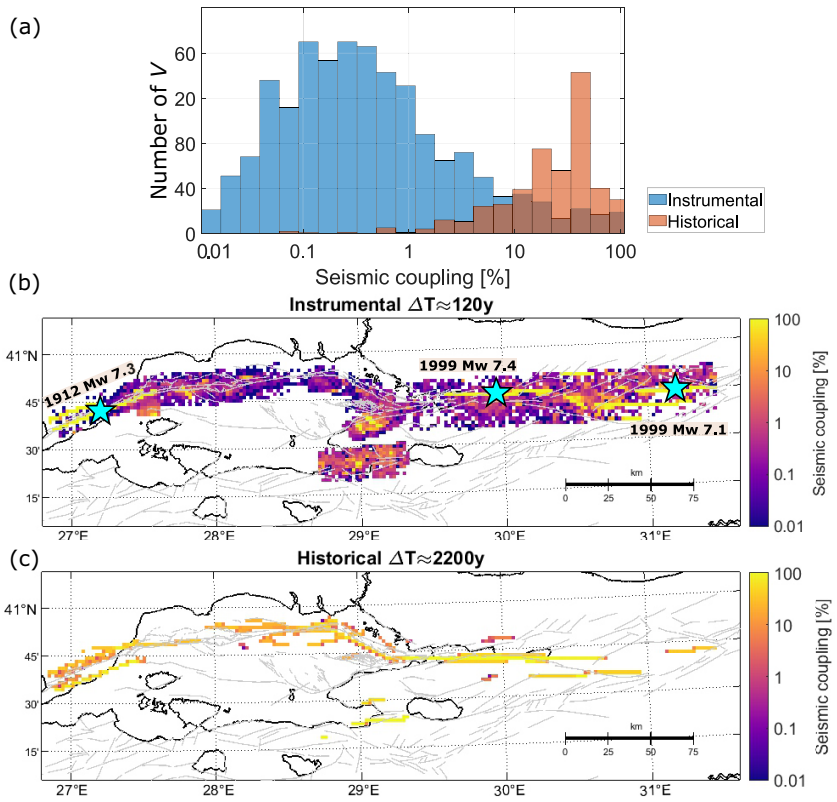

Figure 5: Same as Fig. 4 but for the seismic coupling χ_S estimated from $W_{68\ \text{per cent}}$.

progressive decrease of the $\dot{\varepsilon}_S$ from 13 μstrain yr^{-1} in January 1998 to a minimum of 5 μstrain yr^{-1} in June 1999. This suggests a relative seismic quiescence about 2 months before the large earthquake.

The seismic strain rates reached highest values during the aftershock sequences of the 1999 M_w 7.4 Izmit (5.4×10^{-1} strain yr^{-1}) and 1999 M_w 7.1 Düzce (6.1×10^{-2} strain yr^{-1}) earthquakes. The seismic strain rates follow a similar pattern as the seismicity rates showing an Omori-law type decrease (Bayrak & Öztürk 2004). We note that after the occurrence of a large earthquake, the magnitude of completeness changes through time modifying the total seismic moment estimated from eq. (3). In addition, the time period sampled in each window is not constant, as we used a window of constant number of events. In September 1999, the largest Izmit aftershock with M_w 5.8 occurred in the vicinity of the main shock hypocentre, corresponding to the observable increase of seismic strain rates between the two mainshocks (Fig. 8b). Following the 1999 $M_w > 7$ Izmit–Düzce earthquakes, small increases in the $\dot{\varepsilon}_S$ are observed at the end of year 2000, through 2001 and at the beginning of 2003. Despite these episodic higher rates, the $\dot{\varepsilon}_S$ show a generally decreasing trend until reaching a value closer to the pre-Izmit level about four to 6 yr after the Düzce mainshock.

5 DISCUSSION

Seismic coupling estimates χ_S at the western NAFZ using historical and instrumental seismic catalogues yield significantly different results and display spatial and temporal variations spanning several orders. Using the historical seismicity catalogue, the average χ_S^{hist} is 48% and 96% , depending on the assumed width of the fault zone, indicating that averaged over about nine seismic cycles the relative plate motion along the western NAFZ was almost fully accommodated by large seismic events. The 120 yr covered by the instrumental earthquake catalogue represent about half of the seismic cycle of M 7.5 events in the region (Parsons 2004). The average χ_S^{inst} is <1 per cent, but may locally reach up to 100 per cent (Figs S2 and 5b). Below we discuss how our coupling estimates compare to previous studies, and how the coupling varies in space and time using the high-resolution instrumental catalogue. Finally, we review some of the main limitations of our study, both technical and in terms of the interpretation of the results.

5.1 Comparison with previous estimates of seismic coupling

For the historical time period, the average estimated seismic coupling within the Sea of Marmara is about 48 and 96 per cent assuming that the width of the NAFZ deformation zone is defined by 68 and 95 per cent of the seismicity from the main fault trace, respectively (see Section 4.2, Fig. 5c). This observation is in good agreement with previous estimations from Jenny *et al.* (2004) and Jackson & McKenzie (1988), who found full seismic coupling for this region, obtained from the analysis of two seismic catalogues of 500 and 2550 yr. This suggests that over several seismic cycles, tectonic strain accumulated by plate movement along the western NAFZ is accommodated almost entirely by large seismic events.

In contrast, considering the instrumental time period from 1903 to 2020, Sparacino *et al.* (2022) found seismic coupling <30 per cent on the western portion of the NAFZ, which is much higher than our estimates using the instrumental catalogue. One possible reason behind this discrepancy is that our bins of 2 km × 2 km are substantially smaller than those in their study, leading to several regions not containing large events, which, in turn, leads to an

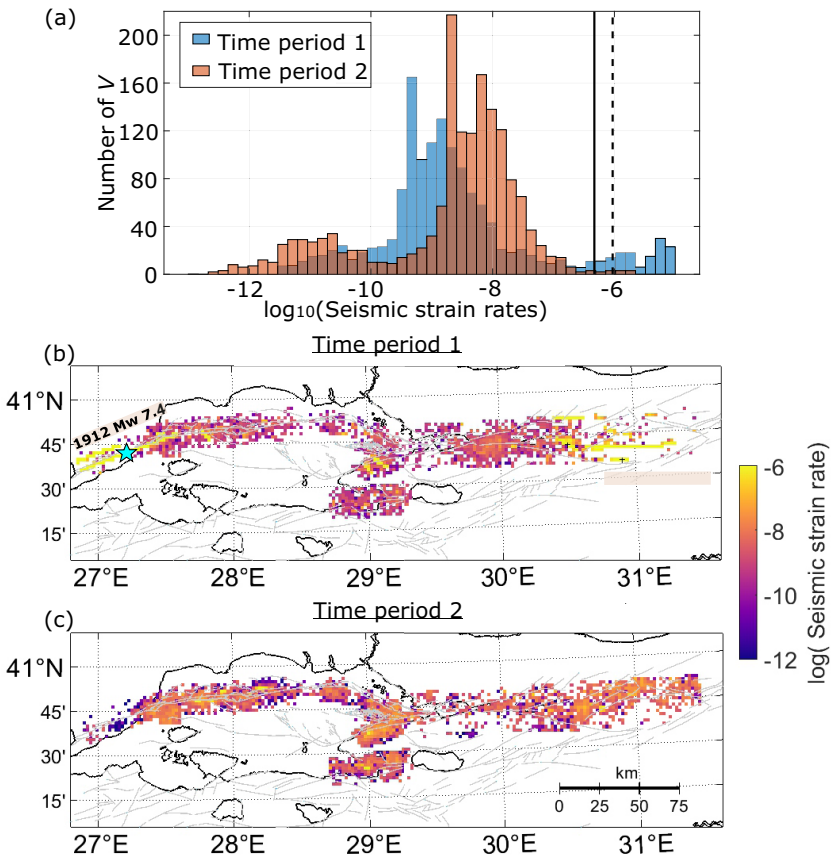

Figure 6: Comparison of seismic strain rates calculated from the instrumental seismicity catalogue for two different time periods before and after the 1999 $M > 7$ Izmit and Düzce earthquakes. (a) Histograms showing seismic strain rates values frequency calculated from 1 January 1900 to 15 August 1999 (the time period 1, blue) and from 1 December 1999 to April 2021 (time period 2, orange). (b) Spatial distribution of seismic strain rates calculated from the instrumental catalogue during time period 1. (c) Same as (b) but for time period 2. The light grey lines indicate mapped faults in the studied area.

overall lower seismic coupling averaged over the different regions (Figs 5b, 7b, c and S5b). This variability among the results suggests that within a single seismic cycle, deformation in the fault zone may be accommodated by any combination of seismic slip, aseismic slip and elastic deformation. For example, selected areas such as the Western High, along the Armutlu peninsula and west of the gulf of Gemlik (Fig. 1 for locations) show a high seismic coupling of up to 100 per cent (Fig. 5).

Several studies discussed the deformation modes of the MMF. Earthquake repeaters have been observed to occur on the Western High and Central Basin, suggesting the occurrence of aseismic slip (Schmittbuhl *et al.* 2016; Bohnhoff *et al.* 2017; Yamamoto *et al.* 2019; Becker *et al.* 2023). At these locations, Becker *et al.* (2023) determined creep rates that might accommodate locally up to 40 per cent of the tectonic deformation. Therefore, the high seismic coupling here obtained for the Western High region suggests that the presence of aseismic deformation in the area is also promoting locally the occurrence of seismicity (e.g. Marsan *et al.* 2017). Furthermore, the full seismic coupling over several seismic cycles obtained with the historical catalogue for the MMF region suggests that large seismic events eventually rupture across segments with varying contributions of aseismic fault creep.

In the case of the Armutlu peninsula, the high seismic coupling recovered with the instrumental catalogue is not surprising as this hydrothermal region is highly active with one of the highest background seismicity rates in the Marmara region extending down to 12 km in depth (Wollin *et al.* 2018; Martínez-Garzón *et al.* 2019). In addition, this segment might have hosted the 1963 M 6.3 earthquake (Pinar *et al.* 2003; Bulut & Aktar 2007). Two large slip transients have been observed in this region with strainmeter recordings (Martínez-Garzón *et al.* 2019; 2021; Durand *et al.* 2022). The observation of such high seismic coupling could indicate that the occurrence of these transients is relatively shallow and hence does not completely release the stress accumulated on the faults, or that the seismicity is also driven by the migration of fluids along the upper crust.

In the Gulf of Gemlik, where no large earthquakes have been reported, the observed high seismic coupling could be explained by the low tectonic strain in this area, which is one of the lowest along the western NAFZ branches (Table 1, eqs 2 and 6).

Outside of these particular regions, we find the highest seismic coupling values (up to 100 per cent using the historical catalogue) in specific regions along the segments that hosted large earthquakes during the 20th century (i.e. the Ganos fault and the Izmit–Düzce rupture). In the case of the Ganos segment, previous studies have inferred a present locking state. Considering the time period from 1903 to 2020, Sparacino *et al.* (2022) determined a seismic coupling between 20 and 30 per cent along the Ganos segment. This discrepancy could suggest that the Ganos fault segment was more active during the time covered in our historical catalogue than during the instrumental period analysed in Sparacino *et al.* (2022).

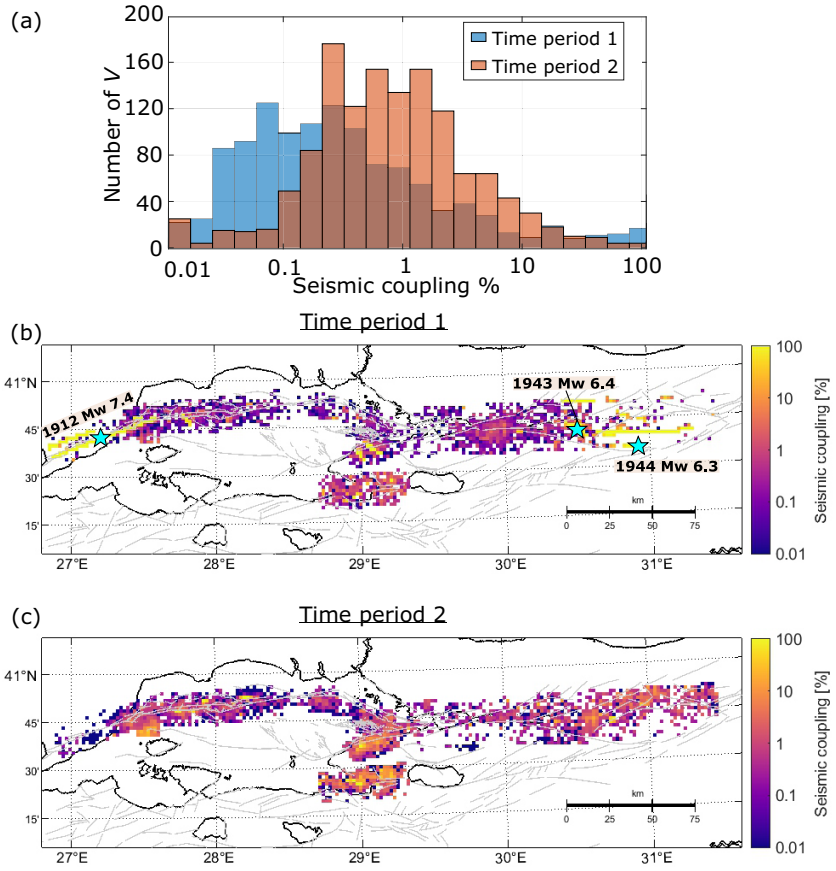

Figure 7: Seismic strain rates as in Fig. 4 converted to seismic coupling using eq. (6).

5.2 Local and regional variations of seismic coupling along the seismic cycle

Our observations show that after the occurrence of local $M > 7$ earthquakes, the seismic coupling in the area surrounding the epicentral region during the subsequent years is lower. Specifically, during time period 2 (from 1 December 1999 to 1 April 2021), the Izmit region shows lower seismic coupling compared to time period 1 (Fig. 7c). A similar behaviour is observed after the 1912 M_w 7.4 Ganos earthquake, in which during the years following this earthquake, there is almost no seismicity recorded around the ruptured segment (e.g. Ergintav *et al.* 2014; Klein *et al.* 2017). This is also in good agreement with the reported fully locked status of the Ganos fault (Motagh *et al.* 2007).

The observation of lower seismic coupling after the occurrence of the large earthquakes around their rupture areas is in good agreement with the post-seismic behaviour following a large earthquake (Wang 2012). When a large earthquake occurs, aseismic deformation typically occurs in the rupture area and its surroundings, including afterslip and post-seismic relaxation (Perfettini & Avouac 2004). Periods of enhanced aseismic slip may follow large events for several years (e.g. Çakir *et al.* 2012; Aslan *et al.* 2019). The aseismic slip after the occurrence of large earthquakes participates in the release of stored elastic strain energy and could temporarily prevent local stress build up, resulting in lower seismicity rates and event magnitudes and consequently, lower seismic coupling. However, it is important to remark that the observed changes in the seismic coupling might be apparent due to the relatively short time period comprised by the data, rather than truly reflecting different behaviour throughout the seismic cycle.

However, at a regional scale, the temporal evolution of seismic coupling from the instrumental seismicity shows that the occurrence of the 1999 M_w 7.4 Izmit and M_w 7.1 Düzce earthquakes resulted in larger seismic strain rates $\dot{\varepsilon}_S$ for most of the Sea of Marmara. One possibility is that this broader effect may be due to stress transfer from the main shocks, possibly resulting in enhanced shear stresses and slip extending towards the west into the Marmara region as fault segments adjacent to the rupture tip were loaded. Stress transfer and fault loading from the occurrence of large earthquakes has been observed to play an important role in activating fault segments towards large earthquakes in the NAFZ and other large faults (Stein *et al.* 1997). Durand *et al.* (2010) mentioned a similar phenomenon, with the activation of several seismicity clusters along the NAFZ following the Izmit earthquake. This was the case along the Armutlu peninsula and the North of Marmara island, where we observed high seismic coupling driven by the occurrence of $M > 5$ earthquakes in the area. Another possibility is that the deformation related to the 1999 Izmit and Düzce earthquakes could have promoted transient deformation extending deeper than the brittle crust into the upper mantle, hence reaching further distances away from the rupture and covering a longer time period (e.g. Ergintav *et al.* 2009; Durand *et al.* 2010).

5.3 Limitations and assumptions included in this study

With our selection of cells covering areas of 2×2 km^2, we are able to retrieve detailed spatio-temporal variations of the seismic coupling.

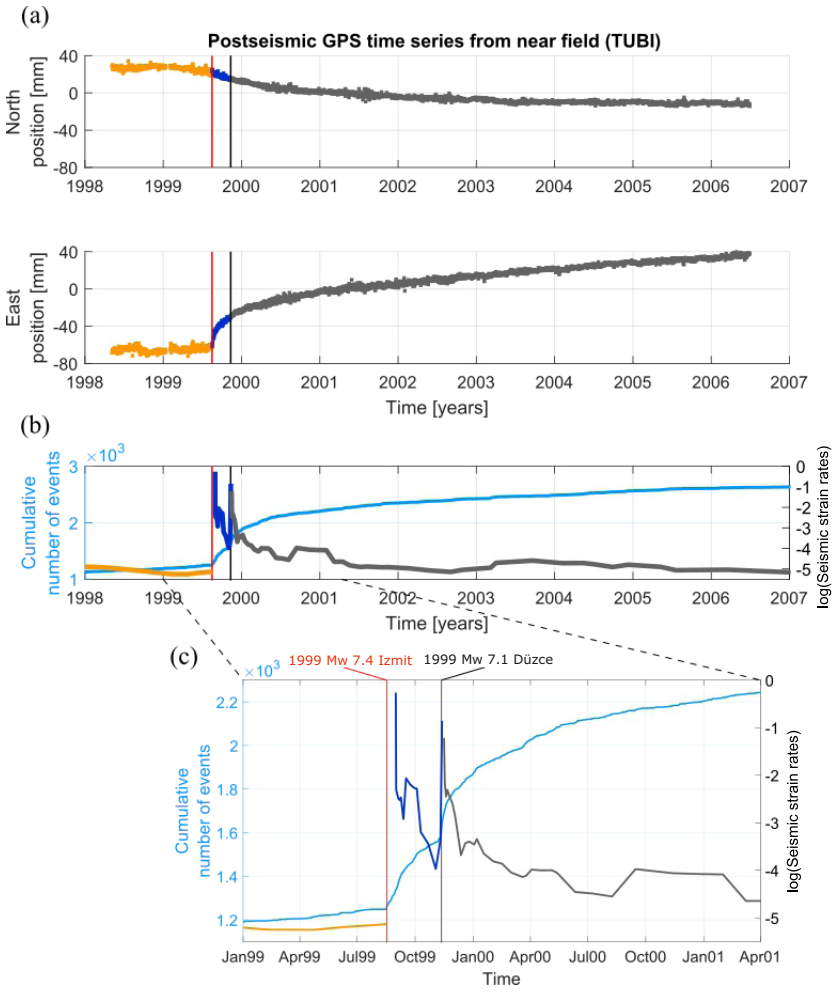

Figure 8: (a) TUBI north and east GPS displacement time-series after correcting coseismic offsets relative to a fixed Eurasian Plate (from Ergintav *et al.* 2009). Red and black vertical lines indicate the 1999 Izmit and Düzce earthquakes, respectively. (b) Long-term seismic strain rates evolution from 1998 to 2007 in the Izmit–Düzce seismic zone for the period before the 1999 M_w 7.4 Izmit earthquakes (yellow), between the 1999 M_w 7.4 Izmit and 1999 M_w 7.1 Düzce earthquakes (blue) and after the 1999 M_w 7.1 Düzce earthquake (grey). The origin times of the 1999 M_w 7.4 Izmit and 1999 M_w 7.1 Düzce earthquakes are represented with vertical red and black lines, respectively. (c) same as (b) but zoom in between January 1999 and April 2001.

This, however, also resulted in observing a broader range of seismic coupling values, which may locally peak to extreme values down to 0.01 per cent and up to 100 per cent. This is different to, for example Sparacino *et al.* (2022) who considered $2^\circ \times 2^\circ$ cells. Jenny *et al.* (2004) calculated the seismic strain rates following the grid used for the geodetic strain field. These cells were non-uniform rectangles with various sizes covering an even larger surface area. Their larger analysis regions result in very few areas not containing seismicity, hence leading typically to larger estimations of the seismic coupling. We note, however, that in our study, the volume sampled by the seismic strain rates (eq. 3) is smaller than the volume sampled by the tectonic strain rates (eq. 2). This is due to the different resolution available for each of the two quantities, as well as their different intrinsic variability. However, since the seismic strain rates and the tectonic strain rates are each divided by the corresponding sampled volume, the errors resulting from this effect should be minor.

Seismic coupling may be estimated using different approaches that may affect the results. For example, Scholz & Campos (2012) utilized the ratio between seismic and geodetic slip rates and Sparacino *et al.* (2022) used the ratio between the corresponding seismic moments. Here, we use the ratio of the seismic and geodetic strain rates to account for the width of the fault damage zone, which is highly variable along the analysed segments.

Within our study, we tested both an instrumental and a historical seismicity catalogue to estimate the seismic strain rates and seismic coupling. The historical catalogue contains earthquakes with $M \geq 5.8$, including numerous large historical earthquakes, but it lacks of small events located on- and off-fault, while the instrumental catalogue includes all magnitudes down to 0.2 and only a few large events such as the 1999 M_w 7.4 Izmit earthquakes and 1999 M_w 7.1 Düzce earthquakes. The high M_C of the historical catalogue signifies a strong deficit from the strain rates of smaller earthquakes. Taking the small events into account would likely imply an increase of the seismic moment release by a factor between 1 and 2 (e.g. McGarr 2014). This increase in the seismic moment would then likely be accommodated on and off- fault, as it is visible with the instrumental catalogue.

The estimation of seismic strain rates is commonly related to the seismicity rates for hazard-estimation purposes (e.g. Zeng *et al.* 2018; Stevens & Avouac 2021). For such applications, it is important that the background seismicity rates are represented, and hence seismicity catalogues are declustered. For our application, however,

this is not essential as we estimated the Kostrov strain rate, where the seismic moment released in each event is summed (eq. 3). As seismic moment increases exponentially with magnitude, the seismic moment release in the aftershock sequences is typically much smaller than that from their corresponding main shock. Hence, declustering the instrumental seismicity catalogue should not result in strong changes in the cumulative seismic moment and Kostrov strain. This is additionally confirmed by our study, where we observe that the majority of accumulated strain is released via larger magnitude earthquakes. Nevertheless, it implies that the seismic energy release promoted by stress transfer is assumed to be part of the seismic energy release driven by the tectonic loading.

6 CONCLUSIONS

We calculated seismic coupling along 14 segments of the North Anatolian Fault Zone in northwestern Türkiye from a 120-yr instrumental and a 2300-yr historical seismicity catalogue. We also investigated spatio-temporal variations of seismic coupling focusing on time periods before and after the 1999 M_w 7.4 Izmit, M_w 7.1 Düzce and 1912 M_w 7.4 Ganos earthquakes. Finally, we compared the evolution of the seismic strain rates in the region of the 1999 $M > 7$ Izmit and Düzce earthquakes between 1998 and 2007 and the post-seismic deformation recorded in geodetic data following these ruptures. Our main conclusions are:

(i) Seismic strain rates derived from the historical catalogue covering approximately 2300 yr are of the same order as geodetic strain rates ($\sim 10^{-7}$ strain yr^{-1}), while estimates from the instrumental catalogue are two orders lower. This discrepancy is likely related to the strong difference in the magnitude ranges included within each of the seismicity catalogues and to their different time spans. The difference in the strain rates estimates between the catalogues suggests that the majority of the accumulated strain is released via large magnitude earthquakes, and that the small seismicity during the interseismic period is not enough to accommodate the plate boundary deformation.

(ii) Over the several (up to 9) seismic cycles covered in the historical catalogue, most of the accumulated tectonic strain near the main fault traces was released seismically. In contrast, the instrumental catalogue reflecting less than one complete seismic cycle shows a deficit in the seismic strain rates. Comparing the seismic coupling from historical catalogues with the one from the instrumental catalogue suggests an ongoing accumulation of strain on the fault to be released seismically via future large earthquakes, rather than the occurrence of aseismic slip.

(iii) The seismic coupling in the Marmara region increased after the 1999 $M > 7$ Izmit and Düzce earthquakes, suggesting that this area could have been loaded by stress transfer from the occurrence of these earthquakes and/or other mechanisms involving long-lasting deformation.

(iv) The seismic coupling decreased after the 1999 $M > 7$ Izmit and 1912 Ganos earthquakes in their coseismic rupture area, suggesting that the faults released a substantial portion of their accumulated strain and that they need time to accumulate elastic strain and generate seismicity. Hence, we observe a local variation of the seismic coupling according to the different stages of the seismic cycle.

(v) Within the Sea of Marmara, the overall seismic coupling retrieved from the instrumental catalogue is of about 48 per cent, illustrating that a significant proportion (52 per cent) of long-term shear strain could be accommodated by aseismic deformation during the instrumental period, or, that the fault is accumulating strain to be released in future large earthquakes. Compared with estimates from the historical catalogue, the second hypothesis seems more likely.

(vi) Around the epicentral regions of the $M > 7$ Izmit and Düzce earthquakes, the temporal evolution of the seismic strain rates following the occurrence of these earthquakes (i.e. including their aftershock sequences) is coherent with the temporal evolution of the post-seismic deformation of the region.

SUPPORTING INFORMATION

Supplementary data are available at *GJI* online.

Please note: Oxford University Press is not responsible for the content or functionality of any supporting materials supplied by the authors. Any queries (other than missing material) should be directed to the corresponding author for the paper.

ACKNOWLEDGMENTS

We thank Semih Ergintav for providing the GPS data and his support in processing them. AA and PM-G acknowledge funding from the Helmholtz Association in the frame of the Helmholtz Young Investigators Group SAIDAN (VH-NG-1323). Time-series from station TUBI shown in Fig. 8 are taken from the Supplementary materials of Ergintav *et al.* (2009).

CONFLICT OF INTEREST

The authors declare no conflict of interest.

DATA AND CODE AVAILABILITY

The KOERI earthquake catalogue starting in 1900 is available from http://www.koeri.boun.edu.tr/sismo/2/earthquake-catalog. None of the used computer codes has been specifically developed for the purpose of this study. For estimation of the seismic coupling, we used MATLAB home-made computer codes based on algorithms existing in the literature.

REFERENCES

Aslan, G. *et al.* 2019. Shallow creep along the 1999 Izmit earthquake rupture (Turkey) from GPS and High temporal resolution interferometric synthetic aperture radar data (2011–2017), *J. geophys. Res.,* **124**(2), 2218–2236.

Barka, A., Akyuz, H.S., Altunel, E.R.H.A.N., Sunal, G., Cakir, Z., Dikbas, A. & Page, W. 2002. The surface rupture and slip distribution of the 17 August 1999 Izmit earthquake (M 7.4), North Anatolian fault, *Bull. seism. Soc. Am.,* **92**(1), 43–60.

Barka, A.A., 1992. The North Anatolian fault zone, *Ann. Tecton.,* **6**(Special issue), 164–195.

Bayrak, Y. & Öztürk, S. 2004. Spatial and temporal variations of the aftershock sequences of the 1999 İzmit and Düzce earthquakes, *Earth, Planets Space,* **56**(10), 933–944.

Becker, D., Martínez-Garzón, P., Wollin, C., Kılıç, T. & Bohnhoff, M. 2023. Variation of fault creep along the overdue Istanbul-Marmara Seismic Gap in NW Türkiye, *Geophys. Res. Lett.,* **50**(6), e2022GL101471, doi:10.1029/2022GL101471.

Ben-Zion, Y. 2008. Collective behavior of earthquakes and faults: continuum-discrete transitions, progressive evolutionary changes, and different dynamic regimes, *Rev. Geophys.,* **46**(4), doi:10.1029/2008RG000260.

BenZion, Y. & Sammis, C.G., 2003. Characterization of fault zones, *PAGEOPH,* **160,** 677–715.

Bohnhoff, M. *et al.*, 2017. Repeating Marmara Sea earthquakes: indication for fault creep, *Geophys. J. Int.,* **210**(1), 332–339.

Bohnhoff, M., Bulut, F., Dresen, G., Malin, P.E., Eken, T. & Aktar, M., 2013. An earthquake gap south of Istanbul, *Nat. Commun.,* **4,** doi:10.1038/ncomms2999.

Bohnhoff, M., Grosser, H. & Dresen, G. 2006. Strain partitioning and stress rotation at the North Anatolian fault zone from aftershock focal mechanisms of the 1999 Izmit M w= 7.4 earthquake, *Geophys. J. Int.,* **166**(1), 373–385.

Bohnhoff, M., Ickrath, M. & Dresen, G. 2016b. Seismicity distribution in conjunction with spatiotemporal variations of coseismic slip and postseismic creep along the combined 1999 Izmit-Düzce rupture, *Tectonophysics,* **686,** 132–145.

Bohnhoff, M., Martínez-Garzón, P., Bulut, F., Stierle, E. & Ben-Zion, Y. 2016a. Maximum earthquake magnitudes along different sections of the North Anatolian fault zone, *Tectonophysics,* **674,** 147–165.

Brune, J.N. 1968. Seismic moment, seismicity and rate of slip along major fault zones, *J. geophys. Res.,* **73,** 777–784.

Bulut, F. & Aktar, M. 2007. Accurate relocation of İzmit earthquake (Mw= 7.4, 1999) aftershocks in Çınarcık Basin using double difference method, *Geophys. Res. Lett.,* **34**(10), doi:10.1029/2007GL029611.

Çakir, Z., Ergintav, S., Özener, H., Dogan, U., Akoglu, A.M., Meghraoui, M. & Reilinger, R. 2012. Onset of aseismic creep on major strike-slip faults, *Geology,* **40**(12), 1115–1118.

Carafa, M.M., Valensise, G. & Bird, P. 2017. Assessing the seismic coupling of shallow continental faults and its impact on seismic hazard estimates: a case-study from Italy, *Geophys. J. Int.,* **209**(1), 32–47.

Cattin, R. & Avouac, J.P. 2000. Modeling mountain building and the seismic cycle in the Himalaya of Nepal, *J. geophys. Res.,* **105**(B6), 13 389–13 407.

Coskun, S., Dondurur, D., Cifci, G., Aydemir, A., Gungor, T. & Drahor, M.G. 2017. Investigation on the tectonic significance of Izmir, Uzunada Fault Zones and other tectonic elements in the Gulf of Izmir, western Turkey, using high resolution seismic data, *Mar. Pet. Geol.,* **83,** 73–83.

Dresen, G., Kwiatek, G., Goebel, T. & Ben-Zion, Y. 2020. Seismic and aseismic preparatory processes before large stick–slip failure, *Pure appl. Geophys.,* **177,** 5741–5760.

Durand, V. *et al.* 2022. Deciphering aseismic deformation along submarine fault branches below the eastern Sea of Marmara (Turkey): insights from seismicity, strainmeter, and GNSS data, *Earth planet. Sci. Lett.,* **594,** doi:10.1016/j.epsl.2022.117702.

Durand, V., Bouchon, M., Karabulut, H., Marsan, D., Schmittbuhl, J., Bouin, M.P. & Daniel, G. 2010. Seismic interaction and delayed triggering along the North Anatolian Fault, *Geophys. Res. Lett.,* **37**(18), doi:10.1029/2010GL044688.

Emre, Ö., Duman, T.Y., Özalp, S., Elmacı, H., Olgun, Ş. & Şaroğlu, F. 2013. Active fault map of Turkey with explanatory text, General Directorate of Mineral Research and Exploration (MTA), Special publication series 30, ISBN: 978-605-5310-56-1.

Ergintav, S. *et al.* 2014. Istanbul's earthquake hot spots: geodetic constraints on strain accumulation along faults in the Marmara seismic gap, *Geophys. Res. Lett.,* **41**(16), 5783–5788.

Ergintav, S., McClusky, S., Hearn, E., Reilinger, R., Cakmak, R., Herring, T. & Tari, E. 2009. Seven years of postseismic deformation following the 1999, M = 7.4 and M = 7.2, Izmit-Düzce, Turkey earthquake sequence, *J. geophys. Res.,* **114**(B7), doi:10.1029/2008JB006021.

Hanks, T.C. & Kanamori, H. 1979. A moment magnitude scale, *J. geophys. Res.,* **84**(B5), 2348–2350.

Hergert, T. & Heidbach, O., 2010. Slip-rate variability and distributed deformation in the Marmara Sea fault system, *Nat. Geosci.,* **3**(2), 132–135.

Jackson, J. & McKenzie, D. 1988. The relationship between plate motions and seismic moment tensors, and the rates of active deformation in the Mediterranean and Middle East, *Geophys. J. Int.,* **93**(1), 45–73.

Janssen, C. *et al.* 2009. Tectonic evolution of the Ganos segment of the North Anatolian Fault (NW Turkey), *J. Struct. Geol.,* **31**(1), 11–28.

Jenny, S., Goes, S., Giardini, D. & Kahle, H.G. 2004. Earthquake recurrence parameters from seismic and geodetic strain rates in the eastern Mediterranean, *Geophys. J. Int.,* **157**(3), 1331–1347.

Jolivet, R. & Frank, W.B. 2020. The transient and intermittent nature of slow slip, *AGU Adv.,* **1**(1), e2019AV000126, doi:10.1029/2019AV000126.

Kadirioğlu, F.T. & Kartal, R.F. 2016. The new empirical magnitude conversion relations using an improved earthquake catalogue for Turkey and its near vicinity (1900-2012), *Turk. J. Earth Sci.,* **25**(4), 300–310.

Karabulut, H., Schmittbuhl, J., Özalaybey, S., Lengline, O., Kömeç-Mutlu, A., Durand, V. & Bouin, M.P. 2011. Evolution of the seismicity in the eastern Marmara Sea a decade before and after the 17 August 1999 Izmit earthquake, *Tectonophysics,* **510**(1-2), 17–27.

Ketin, I., 1948. Über die tektonisch-mechanischen Folgerungen aus den großen anatolischen Erdbeben des letzten Dezenniums, *Geol. Rundsch.,* **36,** 77–83.

Kılıç, T., Ottemöller, L., Havskov, J., Yanık, K., Kılıçarslan, Ö., Alver, F. & Özyazıcıoğlu, M. 2017. Local magnitude scale for earthquakes in Turkey, *J. Seismol.,* **21**(1), 35–46.

Klein, E., Duputel, Z., Masson, F., Yavasoglu, H. & Agram, P. 2017. Aseismic slip and seismogenic coupling in the Marmara Sea: what can we learn from Onland Geodesy?, *Geophys. Res. Lett.,* **44**.3100–3108.

Kostrov, B.V. 1974. Seismic moment and energy of earthquakes, and seismic flow of rock, *Izvest. Acad. Sci. USSR (Phys. Solid Earth),* **1,** 23–40.

Lange, D. *et al.* 2019. Interseismic strain build-up on the submarine North Anatolian Fault offshore Istanbul, *Nat. Commun.,* **10**(1), doi:10.1038/s41467-019-11016-z.

Le Pichon, X., Şengör, A.M.C., Demirbağ, E., Rangin, C., Imren, C., Armijo, R. & Tok, B. 2001. The active main Marmara fault, *Earth planet. Sci. Lett.,* **192**(4), 595–616.

Lindsey, E.O. *et al.* 2021. Slip rate deficit and earthquake potential on shallow megathrusts, *Nat. Geosci.,* **14,** 321–326.

Marsan, D., Bouchon, M., Gardonio, B., Perfettini, H., Socquet, A. & Enescu, B. 2017. Change in seismicity along the Japan trench, 1990–2011, and its relationship with seismic coupling, *J. geophys. Res.,* **122**(6), 4645–4659.

Martínez-Garzón, P. *et al.* 2021. Near-fault monitoring reveals combined seismic and slow activation of a fault branch within the Istanbul–Marmara seismic gap in Northwest Turkey, *Seismol. Res. Lett.,* **92**(6), 3743–3756.

Martínez-Garzón, P. *et al.*, 2019. Slow strain release along the eastern Marmara region offshore Istanbul in conjunction with enhanced local seismic moment release, *Earth planet. Sci. Lett.,* **510,** 209–218.

Mcclusky, S., Balassanian, S., Barka, A., Demir, C., Ergintav, S., Georgiev, I. & Veis, G. 2000. Global Positioning System constraints on plate kinematics and dynamics in the eastern Mediterranean and Caucasus, *J. geophys. Res.,* **105**(B3), 5695–5719.

McGarr, A. 2014. Maximum magnitude earthquakes induced by fluid injection, *J. geophys. Res.,* **119,** 1008–1019.

McLaskey, G.C. & Yamashita, F. 2017. Slow and fast ruptures on a laboratory fault controlled by loading characteristics, *J. geophys. Res.,* **122**(5), 3719–3738.

Meade, B.J., 2005. Block models of crustal motion in southern California constrained by GPS measurements, *J. geophys. Res.,* **110**(B3), doi:10.1029/2004JB003209.

Meghraoui, M., Toussaint, R. & Aksoy, M.E. 2021. The slip deficit on the North Anatolian Fault (Turkey) in the Marmara Sea: insights from paleoseismicity, seismicity and geodetic data, *Mediterran. Geosci. Rev.,* **3**(1), 45–56.

Motagh, M., Hoffmann, J., Kampes, B., Baes, M. & Zschau, J. 2007. Strain accumulation across the Gazikoy–Saros segment of the North Anatolian Fault inferred from Persistent Scatterer Interferometry and GPS measurements, *Earth planet. Sci. Lett.,* **255**(3-4), 432–444.

Murru, M., Akinci, A., Falcone, G., Pucci, S., Console, R. & Parsons, T. 2016. M≥ 7 earthquake rupture forecast and time-dependent probability

for the Sea of Marmara region, Turkey, *J. geophys. Res.,* **121**(4), 2679–2707.

Örgülü, G. 2011. Seismicity and source parameters for small-scale earthquakes along the splays of the North Anatolian Fault (NAF) in the Marmara Sea, *Geophys. J. Int.,* **184**(1), 385–404.

Öztürk, Y.K., Özel, N.M. & Özbakir, A.D. 2015. States of local stresses in the Sea of Marmara through the analysis of large numbers of small earthquakes, *Tectonophysics,* **665,** 37–57.

Pacheco, J.F., Sykes, L.R. & Scholz, C.H. 1993. Nature of seismic coupling along simple plate boundaries of the subduction type, *J. geophys. Res.,* **98,** 14 133–14 159.

Parsons, T., 2004. Recalculated probability of M ≥ 7 earthquakes beneath the Sea of Marmara, Turkey, *J. geophys. Res.,* **109**(B5), doi:10.1029/2003JB002667.

Peng, Z. & Gomberg, J. 2010. An integrated perspective of the continuum between earthquakes and slow-slip phenomena, *Nat. Geosci.,* **3**(9), 599–607.

Perfettini, H. & Avouac, J.-P. 2004. Postseismic relaxation driven by brittle creep: a possible mechanism to reconcile geodetic measurements and the decay rate of aftershocks, application to the Chi-Chi earthquake, Taiwan, *J. geophys. Res.,* **109**(B2), doi:10.1029/2003JB002488.

Pinar, A., Honkura, Y. & Kuge, K. 2001. Seismic activity triggered by the 1999 Izmit earthquake and its implications for the assessment of future seismic risk, *Geophys. J. Int.,* **146**(1), F1–F7.

Pinar, A., Kuge, K. & Honkura, Y. 2003. Moment tensor inversion of recent small to moderate sized earthquakes: implications for seismic hazard and active tectonics beneath the Sea of Marmara, *Geophys. J. Int.,* **153**(1), 133–145.

Radiguet, M., Perfettini, H., Cotte, N., Gualandi, A., Valette, B., Kostoglodov, V. & Campillo, M. 2016. Triggering of the 2014 M w 7.3 Papanoa earthquake by a slow slip event in Guerrero, Mexico, *Nat. Geosci.,* **9**(11), 829–833.

Reid, H.F. 1910. The mechanics of the earthquake, vol. II of the California earthquake of April 18, 1906, Report of the State Investigation Commission, Carnegie Institution of Washington, Washington DC (reprinted 1969).

Reilinger, R. *et al.*, 2006. GPS constraints on continental deformation in the Africa– Arabia–Eurasia continental collision zone and implications for the dynamics of plate interactions, *J. geophys. Res.,* **111**(B5), doi:10.1029/2005JB004051.

Romanet, P., Bhat, H.S., Jolivet, R. & Madariaga, R. 2018. Fast and slow slip events emerge due to fault geometrical complexity, *Geophys. Res. Lett.,* **45**(10), 4809–4819.

Sakic, P., Piété, H., Ballu, V., Royer, J.-Y., Kopp, H., Lange, D., *et al.* 2016. No significant steady state surface creep along the North Anatolian Fault offshore Istanbul: Results of 6 months of seafloor acoustic ranging. *Geophysical Research Letters,* **43**(13), 2016GL069600. https://doi.org/10.1002/2016GL069600.

Savage, J.C., 1983. A dislocation model of strain accumulation and release at a subduction zone, *J. geophys. Res.,* **88,** 4984–4996.

Schmittbuhl, J., Karabulut, H., Lengliné, O. & Bouchon, M. 2015. Seismicity distribution and locking depth along the main Marmara Fault, Turkey, *Geochem. Geophys. Geosyst.,* **17,** 954–965.

Schmittbuhl, J., Karabulut, H., Lengliné, O. & Bouchon, M. 2016. Long-lasting seismic repeaters in the Central Basin of the Main Marmara Fault, *Geophys. Res. Lett.,* **43**(18), 9527–9534.

Scholz, C.H. & Campos, J. 1995. On the mechanism of seismic decoupling and back-arc spreading in subduction zones, *J. geophys. Res.,* **100,** 22 103–22 115.

Scholz, C.H. & Campos, J. 2012. The seismic coupling of subduction zones revisited, *J. geophys. Res.,* **117**(B5), doi:10.1029/2011JB009003.

Scordilis, E.M. 2006. Empirical global relations converting MS and Mb to moment magnitude, *J. Seismol.,* **10,** 225–236.

Sieh, K. *et al.* 2008. Earthquake supercycles inferred from sea-level changes recorded in the Corals of West Sumatra, *Science,* **322**(5908), 1674–1678.

Sparacino, F., Galuzzi, B.G., Palano, M., Segou, M. & Chiarabba, C. 2022. Seismic coupling for the Aegean-Anatolian region, *Earth Sci. Rev.,* **228,** doi:10.1016/j.earscirev.2022.103993.

Stein, R.S., Barka, A.A. & Dieterich, J.H. 1997. Progressive failure on the North Anatolian fault since 1939 by earthquake stress triggering, *Geophys. J. Int.,* **128**(3), 594–604.

Stevens, V. L. & Avouac, J.-P.. 2021. On the relationship between strain rate and seismicity in the India–Asia collision zone: implications for probabilistic seismic hazard. *Geophysical Journal International,* **226**(1), 220–245. https://doi.org/10.1093/gji/ggab098.

Thatcher, W. & Rundle, J.B. 1979. A model for the earthquake cycle in underthrust zones, *J. geophys. Res.,* **84,** 5540–5556.

Uchida, N., Kalafat, D., Pinar, A. & Yamamoto, Y. 2019. Repeating earthquakes and interplate coupling along the western part of the North Anatolian Fault, *Tectonophysics,* **769,** doi:10.1016/j.tecto.2019.228185.

Wang, K., Hu, Y. & He, J. 2012. Deformation cycles of subduction earthquakes in a viscoelastic Earth, *Nature,* **484**(7394), 327–332.

Ward, S.N. 1998. On the consistency of earthquake moment release and space geodetic strain rates: Europe, *Geophys. J. Int.,* **135**(3), 1011–1018.

Wells, D.L. & Coppersmith, K.J., 1994. New empirical relationships among magnitude, rupture length, rupture width, rupture area, and surface displacement, *Bull. seism. Soc. Am.,* **84**(4), 974–1002.

Wollin, C., Bohnhoff, M., Martínez-Garzón, P., Ku¨perkoch, L. & Raub, C., 2018. A unified earthquake catalogue for the Sea of Marmara Region, Turkey, based on automatized phase picking and traveltime inversion: seismotectonic implications, *Tectonophysics,* **747–748,** 416–444.

Yamamoto, R. *et al.*, 2019. Seafloor geodesy revealed partial creep of the North Anatolian Fault submerged in the Sea of Marmara, *Geophys. Res. Lett.,* **46**(3), 1268–1275.

Zeng, Y., Petersen, M. D. & Shen, Z.-K. 2018. Earthquake Potential in California-Nevada Implied by Correlation of Strain Rate and Seismicity. *Geophysical Research Letters,* **45**(4), 1778–1785. https://doi.org/10.1002/2017GL075967.